BUBBLE-GATE FOR IN-PLANE FLOW CONTROL IN MICROFLUIDIC CHANNELS

Ali Oskooei[1], Axel Günther[1,2]
[1]*Department of Mechanical and Industrial Engineering,*
[2]*Institute of Biomaterials and Biomedical Engineering, University of Toronto, Canada*

ABSTRACT

We introduce the microfluidic "bubble gate" as a readily implementable strategy for on-chip liquid handling that requires a footprint of only 500 μm × 500 μm and is compliant with single-layer soft lithography. The key active component of the bubble gate is an air bubble that is propelled with an externally applied pressure to either enable or prevent liquid flow through a fluidic gate. We use microscale particle image velocimetry (μPIV) to quantify the transient liquid flow through the bubble gates that were fabricated in polydimethylsiloxane (PDMS) substrates with either ethanol or the biological buffer 3-(N-morpholino) propanesulfonic acid (MOPS) as the working liquids. We demonstrate the dynamic control of bubble gates, their predictable opening and closing in response to a sudden change in the actuation pressure and quantify the resulting bubble displacement. We report a dimensionless operating pressure envelope for the bubble gate that is supported by the results obtained for both working liquids and by a theoretical prediction. We provide different illustrations of the utility of the demonstrated bubble gates.

KEYWORDS

Flow control, well-based microfluidics, micro valves, valving, liquid sampling

INTRODUCTION

Unique characteristics of microfluidic systems are associated with their capacity to controllably manipulate and analyze minute volumes of reagents. To achieve precise control of samples and reagents, readily implementable and effective flow control strategies are needed. Many flow control techniques and micro valve structures that been proposed since the advent of MEMS and lab-on-a-chip systems [1-4]. The previously proposed techniques have relied on a variety of physical phenomena to achieve flow control. The physical phenomena employed for flow control range from optics to electrokinetics and from pneumatics to piezoelectric effect and even phase change and two phase flow [1-4]. While each of the proposed micro valves have shown promise for certain applications, most of them require complex multilayer fabrication or high voltage connections, high temperature gradients, electrochemical reactions or other intrusive phenomena that makes them unsuitable for many applications dealing with sensitive reagents (e.g. biological analysis). Remarkably, despite the many complex solutions, the simplest designs have become most popular. However, their reliance on a very limited choice of (elastomeric) substrate materials, particularly PDMS, provides a key practical challenge.

We introduce a bubble-propelled flow control strategy that we call "bubble gate". The bubble gate requires only a single feature layer, is compliant with different substrate materials (e.g. PDMS, glass, silicon and PMMA), common microfabrication procedures and a small footprint. Gas bubbles have been previously used as active elements in reversible volume-displacing microfluidic actuators [1, 2]. Bubble-assisted flow control does not require complex fabrication procedures and the bubbles have the ability of conforming to different channel geometries. Our bubble gates provide for effective flow control while not requiring any heating or phase change.

The bubble gate is most suitable for well-based integrated microfluidic systems where the liquid samples are delivered to the microchannels via pressurized reservoirs (i.e. wells) similar to the schematics in figure 1a. This method of liquid delivery will eliminate the need for the common bulky syringe pumps and allows the outgoing liquid to be sampled at the outlet using the same bubble gate flow control. The bubble gate is also scalable and readily implementable in multilayer structures as will be shown in the following sections.

EXPERIMENT

Figure 1b illustrates the design and mechanism of action for the bubble gate. In this strategy, flow control is achieved by means of a computer controlled gas stream that intercepts a liquid stream at a T-junction, forming a long bubble. Closely positioned micropillars are employed to confine the bubble motion. The bubble breaks into the liquid stream and occupies the entire liquid cross-section, when the gas pressure is maintained, hence, blocking the liquid flow. The bubble gate's operation can be divided to three key states: 1) when the bubble is moving into the liquid channel closing the gate (see figure 1b) 2) the fully closed position where the bubble is occupying the entire chamber made by the liquid channel walls and the micropillars (see figure 1b) 3) when the bubble is withdrawing from the chamber hence opening the gate. These states define the bubble gate's operation envelope. For the bubble gate to break into the stop valve the pressure difference across the stop valve must be

978-0-9798064-5-2/μTAS 2012/$20©12CBMS-0001

greater than the surface tension pressure or $P_{Gas} - P_{Gate} \geq 2\gamma/d_{Stopvalve}$, where γ is the surface tension coefficient. Substituting for P_{Gate}, the liquid pressure at the gate (see figure 2b), in terms of the liquid pressure head,P_{Liquid}, the gate closing constraint is obtained as $P_{Gas} - (R_2\ P_{Liquid})/(R_1 + R_2) \geq 2\gamma/d_{Stopvalve}$. On the other hand, to prevent bubble break up into the liquid channel when the gate is closed the gas pressure must remain below the surface tension pressure across the micropillars or $P_{Gas} \leq \Delta P_{Pillar} = 2\gamma/d_{Pillar}$. The two aforementioned constraints define the theoretical boundaries for effective bubble gate operation.

Figure 2c shows the normalized operating pressure data validated against the theoretical constraints discussed above. All pressures and constraints are normalized with respect to $\Delta P_{Pillar} = 2\gamma/d_{Pillar}$. The experimental data were obtained for a PDMS made devices with $d_{Pillar} = 20\mu m$ and stop valve entrance width of $d_{Stopvalve} = 75\mu m$. The working liquids employed were ethanol and MOPS buffer. As seen in the figure the experimental data fall well within the operating envelope defined by theory.

To verify the bubble gate's robustness, the bubble gate was opened and closed with a frequency of 0.5 Hz (i.e. 1(sec) open and 1(sec) closed) for 24 hours. Twenty images with frame rate of 3fps were recorded every 30 minutes to ensure and quantify the bubble-gate's extended operation by counting the number of completed cycles in every 20 frames captured for over 24 hours without interruption. The bubble gate did not follow the control signal in less than 10% of the measurements. The lack of responsiveness can be attributed to pressure fluctuations and interface pinning.

Figure 3a shows the bubble gate's effectiveness in blocking liquid flow based on velocity fields obtained by µPIV when the bubble gate is open and closed. To study the bubble gate's dynamic behavior, the bubble gate was subjected to a square wave pressure input with frequencies of *f=0.5* and *f=1*. Figure 3b shows the schematic for the control signal and the mid and full cycle times, t_1 and t_2. Figures 3c, d show the bubble gate's normalized input pressure and displacement in response to the square wave control input. The histograms in figures 3e and 3f quantify repeatability of the cycles using probability distributions of the normalized characteristic times, t_1^* and t_2^*. The competition between the liquid and gas streams is a major source of instability in the bubble movement in high liquid pressure conditions and as a result a wider probability distribution (i.e. red histograms) as compared with lower liquid pressure cases.

To illustrate the bubble gates' function as a sampling tool two experiments were performed. Figures 4a, b show a well-based device with two inlets connected to two pressurized ethanol reservoirs (i.e. wells) one labeled with a fluorescent marker. The inlet channels flow downstream past two bubble gates into a third channel at a Y junction. The bubble gates were alternated with a time delay of three seconds and the downstream concentration response was recorded which is plotted in figure 4c. The "closed" and "open" times were extracted from the concentration distribution in figure 4c and it is concluded that the concentration distribution followed the control signal with negligible deviation as demonstrated by the very narrow histograms in figure 4d.

The bubble gate strategy was also used for liquid sampling in a three layer microfluidic device as shown in figure 4e. The device consisted of three microchannels each on a separate layer with a common inlet and outlet for all channels and individual bubble gates controlling the liquid flow in each layer. Each bubble gate had a separate gas inlet and was controlled independently. Similar to the sampling experiment in figure 4a, pressure head of 0.23 psi was applied to drive the liquid into the channels (resulting in a flow rate of approximately 21µL/min). P_{Closed} was varied between 0.3 and 0.35 psi and P_{Open} was varied between 0.15 and 0.2 psi during the experiment. The fluorescent images in figure 4e show the bubble gate in each layer blocking the flow of the fluorescently labeled liquid in that layer while it flows in the other layers.

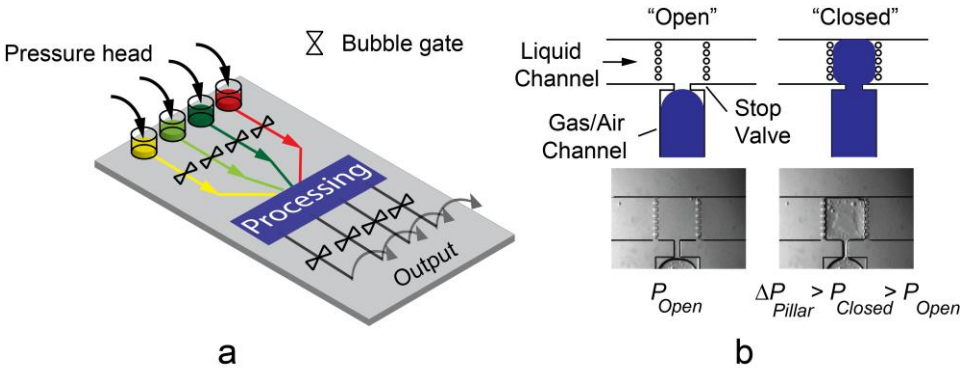

Figure 1 (a) Schematic illustration of a microfluidic device with pressurized wells at the inlet and bubble gates to control sample delivery at the inlet. (b) Schematics of the bubble gate in "open" and "closed" positions.

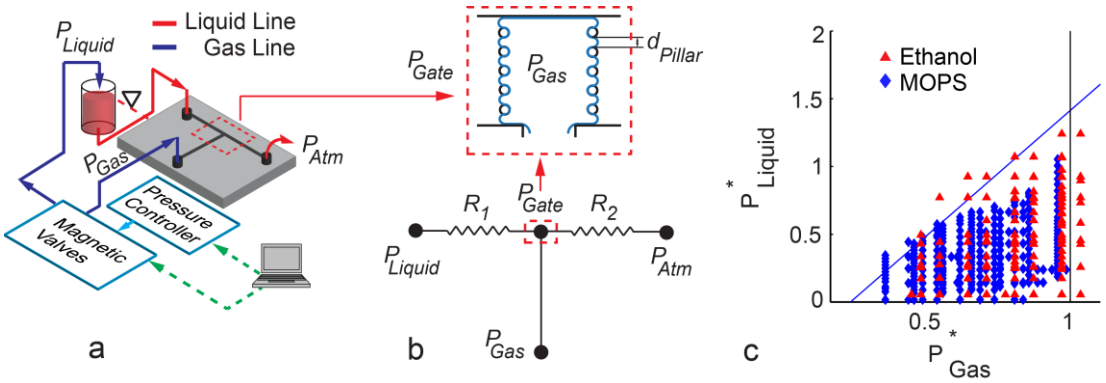

Figure 2 (a) Schematic representation of the experimental setup and (b) the pressure circuit for the bubble gate (c) Measured operating pressure envelopes for the working liquids ethanol (red) and the biological buffer (MOPS, blue). Lines represent the theoretical operational constraints discussed in the text.

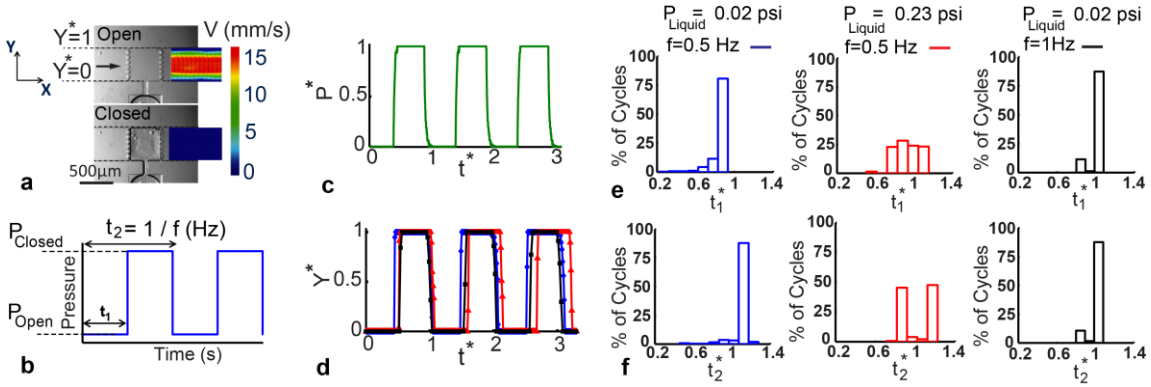

Figure 3 (a) PIV data for the bubble gate in its "open" and "closed" positions. Working fluids are ethanol and air. (b)Schematic illustration of the control signal. (c) Normalized measured gas pressure input vs. time. (d)Normalized bubble displacement vs. time. (e,f) Histograms of normalized t_1 (open time) and normalized t_2 (full cycle).

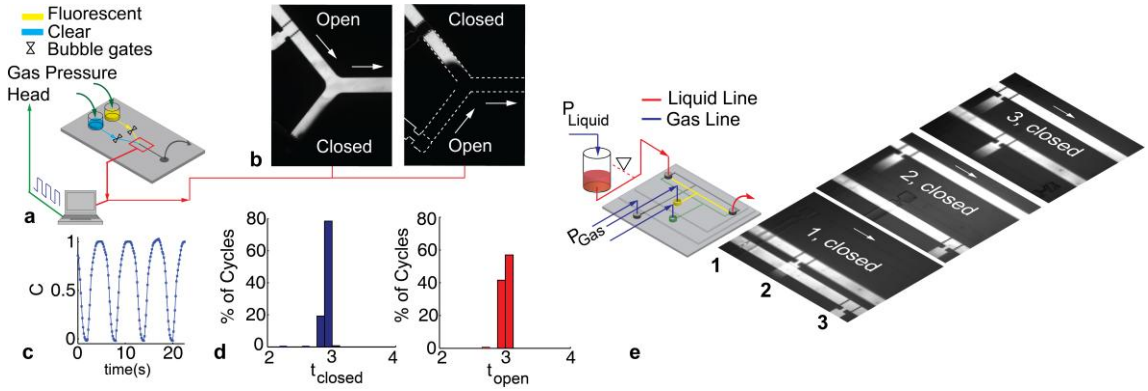

Figure 4 (a) Experimental setup for the Y-channel liquid sampling experiment. (b) Fluorescent images of the Y-channel at open and closed positions.(c) Plot of fluorescence intensity versus time. (d) Histograms for the time each valve is open or closed (e) Schematic illustration for a three-layer device with liquid sampling enabled by bubble gates in all layers. Fluorescent images illustrate the independent operation of the three bubble gates.

REFERENCES

[1] A. K. Au, H. Lai, B. R. Utela and A. Folch, *Microvalves and Micropumps for BioMEMS*, Micromachines, 2011, 2, pp. 179-220.

[2] K. W. Oh and C. H. Ahn, *A review of microvalves*, J. Micromech. Microeng., 2006, 16, pp. R13–R39

[3] C. Zhang, D. Xing, Y. Li, *Micropumps, microvalves, and micromixers within PCR microfluidic chips: Advances and trends*, Biotechnology Advances, 2007, 25, pp. 483–514

[4] D. J. Laser and J. G. Santiago, *A review of micropumps*, J. Micromech. Microeng., 2004, 14, pp. R35–R64.

CONTACT

Axel Guenther, axel.guenther@utoronto.ca.